Nano Energy (2016) 20, 305–314

Available online at www.sciencedirect.com

ScienceDirect

journal homepage: www.elsevier.com/locate/nanoenergy

COMMUNICATION

Multi-yolk-shell copper oxide@carbon octahedra as high-stability anodes for lithium-ion batteries

Tao Chen[a], Yi Hu[a], Baorui Cheng[a], Renpeng Chen[a], Hongling Lv[a], Lianbo Ma[a], Guoyin Zhu[a], Yanrong Wang[a], Changzeng Yan[a], Zuoxiu Tie[a], Zhong Jin[a,*], Jie Liu[a,b,**]

[a]*Key Laboratory of Mesoscopic Chemistry of MOE and Collaborative Innovation Center of Chemistry for Life Sciences, School of Chemistry and Chemical Engineering, Nanjing University, Nanjing 210093, China*
[b]*Department of Chemistry, Duke University, Durham, NC 27708, USA*

Received 14 August 2015; received in revised form 14 December 2015; accepted 24 December 2015
Available online 31 December 2015

KEYWORDS
Multi-yolk-shell octahedra;
Copper oxide;
Metal organic frameworks;
Anode materials;
Lithium-ion batteries

Abstract
Although transition metal oxides have attracted considerable attention for their high energy density as anode materials of lithium-ion batteries, they suffer from large volume expansion during lithiation process, which usually causes fast capacity degradation. Herein, we report a rational design and facile preparation strategy of copper oxide encapsulated mesoporous carbon multi-yolk-shell octahedra, in which multiple CuO nanoparticles are well-confined in the compartments of micro-scale octahedral carbon scaffolds. The advantages of the novel multi-yolk-shell design are that the three-dimensional carbon scaffolds can buffer the volume change and prevent aggregation of CuO nanoparticles during the charge/discharge cycles, provide pathways for electron transport and Li^+ diffusion, and restrict the thin solid-electrolyte interphase layer to the outer surface of carbon shells. The results demonstrate how the electrochemical properties of anodes can be significantly improved by the multi-yolk-shell nanostructures with greatly enhanced structural stability and electrochemical actuation. Moreover, the micrometer-size CuO@C octahedra reduce the relative quality of SEI, resulting in high Coulombic efficiency and long cycling stability. In Li-ion cells, the CuO@C multi-yolk-shell octahedra anodes deliver a highly-reversible capacity of 598 mA h g^{-1} at 250 mA g^{-1}, excellent rate capacity of 365 mA h g^{-1} at 3000 mA g^{-1} and exhibit long-term cyclability with a capacity of 512 mA h g^{-1} after 300 cycles at 500 mA g^{-1}.

*Corresponding author.
**Corresponding author at: Key Laboratory of Mesoscopic Chemistry of MOE and Collaborative Innovation Center of Chemistry for Life Sciences, School of Chemistry and Chemical Engineering, Nanjing University, Nanjing 210093, China.
E-mail addresses: zhongjin@nju.edu.cn (Z. Jin), j.liu@duke.edu (J. Liu).

http://dx.doi.org/10.1016/j.nanoen.2015.12.024
2211-2855/

Introduction

Owing to the high energy density and long cycle life, lithium-ion batteries (LIBs) have been intensively used in portable electronics, electric vehicles, renewable energy systems and smart grids [1-3]. To satisfy the enormous demands of wearable consumer electronics, a new generation of electrode materials with higher capacity, cyclability and rate performance is required. Compared with conventional graphite anodes, transition metal oxides (TMOs) such as copper oxide (CuO), iron oxide, cobalt oxide, manganese oxide, etc., have been viewed as promising anode materials for next generation LIBs owing to their high theoretical capacity [4-7]. Among them, CuO is noteworthy due to its high earth abundance, cost effectiveness, low toxicity and high theoretical capacity of 674 mA h g^{-1} [8]. However, CuO nanomaterials usually suffer from capacity fading and poor cycling life during lithiation/delithiation processes. These disadvantages are caused by low electrical conductivity and large volume expansion. To circumvent these issues, great efforts have been made to enhance the performance of CuO anode electrodes [9-13].

Motivated by their high specific surface areas and tunable pore structures, metal-organic frameworks (MOFs) have been used as sacrificial templates or precursors to form unique porous nanostructures for the applications in energy storage field [14-17]. For examples, Fe_2O_3 [18], CuO [19], CuO/Cu_2O [20], $Zn_xCo_{3-x}O_4$ [21], and $ZnO/ZnFe_2O_4/C$ [22] porous nanoarchitectures have been prepared by using suitable MOF precursors, exhibiting good electrochemical performance as anode materials for LIBs. It is well known that the morphology and architecture of nanostructured materials originated from the synthesis process have significant impacts on the electrochemical performance. An ideal nanostructured electrode should have a three-dimensional (3D) porous architecture encapsulated with nanosized electrochemically-active building blocks, which can reduce the formation of the SEI layer and shorten the distance of Li^+ diffusion [22]. Coincidentally, the multi-yolk-shell not only possesses nanometer-sized subunits that can provide high specific capacity and outstanding rate capability, but also has a stable 3D porous octahedral microstructure for excellent cycling stability. Therefore, rationally designed yolk-shell nanostructures with conductive carbon shells can solve some crucial issues of anode materials, such as large volume variation and low electric conductivity, attributed to their enhanced structural integrity, high stability of solid-electrolyte interphase (SEI) films and electrochemical actuation. Recently, the synthesis of MnO_2@C [23], Fe_3O_4@-Fe_3C [24] and FeO_x@C [25] yolk-shell nanostructures has been reported to improve the cycle life of LIBs. Moreover, Si@C yolk-shell architectures also have been studied to accommodate the large volume expansion of Si-based anode materials during cycling [26-29]. Nevertheless, it still remains a great challenge to design delicate multi-yolk-shell nanostructures with numerous electrochemical-active nanoparticles encapsulated in 3D porous conductive nano-scaffolds to remarkably improve the electrochemical performance of TMO anodes.

Here we demonstrate that a novel CuO@C multi-yolk-shell octahedral nanostructure can be obtained by using Cu-based MOFs as template. To the best of our knowledge, this is the first report on the preparation of TMO-based multi-yolk-shell octahedra for improving lithium storage performance. The synthesis process involves a simple solvothermal process to obtain MOF precursors followed by thermal treatment in N_2 and then in air. Multiple CuO nanoparticles were encapsulated in the compartments of micro-scale carbon nano-octahedra. Compared with the reported porous CuO and CuO/Cu_2O polyhedrons [19,20,30], the architecture of CuO@C multi-yolk-shell octahedra have the following advantages: (1) the conductive carbon octahedral scaffold can restrict the formation of the SEI layer; (2) the stable multi-yolk-shell structure strongly confines the CuO nanoparticles in the carbon octahedra, resulting in a high utilization efficiency of active material CuO; (3) the porous carbon layer between CuO nanoparticles can buffer the volume change, prevent aggregation of CuO nanoparticles, and also provide unobstructed pathways for electron transport and Li^+ diffusion during charge/discharge processes. As a consequence, the novel CuO@C multi-yolk-shell electrodes can deliver very high reversible capacity, rate capacity and long cycling life for lithium storage.

Experimental

Chemicals

Polyvinylpyrrolidone (PVP, M.W. 40,000), $Cu(NO_3)_2 \cdot 3H_2O$ (99.5%), and 1,3,5-benzenetricarboxylic acid (H_3btc, 98%) were purchased from Sigma-Aldrich. N, N-dimethylformamide (DMF) and ethanol were purchased from Sinopharm Chemical Reagent Co., Ltd.

Synthesis of the CuO@C multi-yolk-shell octahedra

Typically, 17.2 mmol of $Cu(NO_3)_2 \cdot 3H_2O$ was dissolved in 30 mL of deionized water. A solution of 1,3,5-benzenetricarboxylic acid (9.6 mmol) in a co-solvent of DMF and ethanol (60 mL, 1:1 by volume) was mixed with 4.0 g of PVP under continuous stirring. After complete dispersion of the reactants, the two solutions were mixed directly. Subsequently, the mixed solution was stirred for 15 min and transferred into a 100 mL Teflon-lined stainless steel autoclave. The autoclave was heated at 100 °C for 10 h. The product was collected and washed with 100 mL ethanol for 3 times. The as-obtained product was called as $Cu_3(btc)_2$ MOF/PVP-*4*. Similarly, for the preparation of $Cu_3(btc)_2$ MOF/PVP-*2* and pristine $Cu_3(btc)_2$ MOFs without PVP, the same procedures were conducted except that the weights of added PVP were 2.0 g and 0 g, respectively. The as-prepared $Cu_3(btc)_2$ MOF/PVP-*4* was carbonized at 700 °C at a heating rate of 2 °C min^{-1} for 4 h in N_2 (99.999%), and then annealed in air at 350 °C for 1 h. To obtain bare CuO octahedra, the $Cu_3(btc)_2$ MOF/PVP-*4* precursor was directly calcined at 500 °C in air for 1 h instead.

Material characterizations

The morphology of samples was characterized by scanning electron microscopy (SEM, HITACH S-4800) and transmission electron microscopy (TEM, JEM-2100). Elemental analysis was performed using energy-dispersive X-ray spectroscopy (EDX) equipped in the SEM. Nitrogen sorption isotherms were

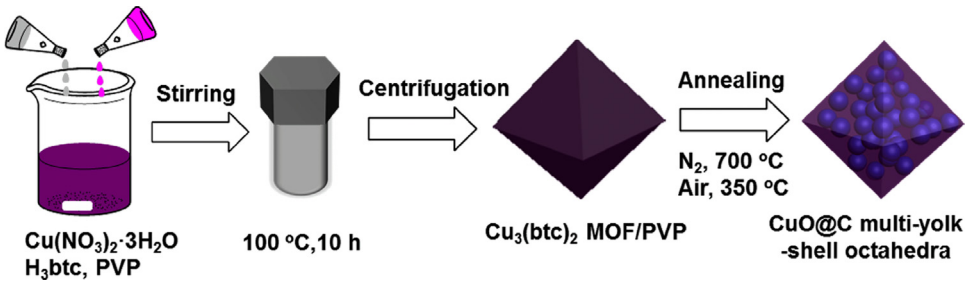

Scheme 1 Schematic illustration for the preparation process of CuO@C multi-yolk-shell octahedra.

obtained through Brunauer–Emmett–Teller (BET) analysis at 77 K on a Micromeritics ASAP-2020. X-ray powder diffraction (XRD) spectra were recorded using a XRD-6000 diffractometer (Shimadzu Co., Japan), equipped with a rotating anode and a Cu Kα radiation source (λ=1.54178 Å). Thermo-gravimetric analysis (TGA) was carried out using a Mettler SDTA851e analyzer at a heating rate of 10 °C min^{-1} in air. Raman spectra were collected using a Renishaw InVia Raman microscope system with an excitation laser of 514 nm wavelength. X-ray photoelectron spectra (XPS) were obtained using a PHI-5000 VersaProbe X-ray photoelectron spectrometer with an Al Kα X-ray radiation.

Electrochemical measurements

The working electrodes were fabricated with the as-prepared active materials, conducting acetylene black, and polyvinylidene fluoride (PVDF) in N-methyl-2-pyrrolidinone (NMP) solvent with a weight ratio of 80:10:10. The slurry was then smeared on a Cu foil and dried in vacuum at 80 °C for 12 h. The assembly of coin cells was performed in an argon-filled glove box by using CR 2032 coin-type cells with lithium foils as counter electrodes, Celgard 2400 membranes as separators, and 1.0 M $LiPF_6$ in a co-solvent of ethylene carbonate and dimethyl carbonate (1:1 by volume) as electrolyte. The galvanostatic charge-discharge performances were measured on a LAND CT2001A multichannel battery test system between 0.01 and 3.0 V at room temperature. The specific capacity was calculated based on the total weight of active materials. The cyclic voltammetry (CV) and electrochemical impendence spectroscopy (EIS) measurements were carried out on a Chenhua CHI-760 electrochemical workstation.

For the tests of full Li-ion cells, cathodes based on commercially-available $LiFePO_4$ (MTI Corp.) were used instead of lithium foils. The $LiFePO_4$ cathodes were prepared by mixing 80 wt% of commercial $LiFePO_4$ powder, 10 wt% of conducting acetylene black and 10 wt% of PVDF binder in NMP, and then the mixed slurry was spread on an Al foil and dried in vacuum at 110 °C for 12 h. Prior to assembling the full cell, the CuO@C multi-yolk-shell octahedra electrode was treated by a simple ex-situ prelithiated process in order to decrease the high initial irreversible capacity [31]. Firstly, the CuO@C multi-yolk-shell octahedra electrode was fully contacted with a lithium foil, and then wetted by the electrolyte solution (1.0 M $LiPF_6$). The loading mass of CuO@C multi-yolk-shell octahedra anodes and $LiFePO_4$ cathodes were ca. 0.5 – 0.6 mg and ca. 1.6 – 2.0 mg, respectively. The as-prepared full cells were cycled between 0.9 V and 4.0 V.

Results and discussion

The synthesis of the CuO@C multi-yolk-shell octahedra is described in Scheme 1. All the synthetic procedures, characterizations and electrochemical measurements involved in this work are described in detail in the Supporting Information. A thermosolvent reaction of H_3btc and Cu^{2+} ions in a mixed water/ethanol solution in the presence of PVP was utilized for the synthesis of $Cu_3(btc)_2$ MOF/PVP-*n*, where the *n* represents the amount of PVP added in the reaction. The morphology of the $Cu_3(btc)_2$ MOF/PVP-*n* was characterized by SEM, as shown in Figure S1. The SEM images of $Cu_3(btc)_2$ MOF/PVP-*4* (Figure S1a and b) present a large number of octahedra with smooth surface and an average edge length of ~2 μm. The as-prepared $Cu_3(btc)_2$ MOF/PVP-*4* octahedra were annealed at 700 °C in N_2 atmosphere with a heating rate of 2 °C min^{-1} for 4 h and then followed by further calcination at 350 °C in air for 1 h to obtain the porous CuO@C multi-yolk-shell octahedra.

The morphologic features of as-prepared CuO@C multi-yolk-shell octahedra are shown in Figure 1. The surface of CuO@C octahedra (Figure 1a and b) became more rugged than original $Cu_3(btc)_2$ MOF/PVP-*4*, owing to the formation of CuO nanoparticles in the octahedra after thermal treatments. The particles attached on the surface of the CuO@C octahedra should be carbon, which are derived from the annealing of MOFs under argon (Figure S2). Interestingly, the general appearance of the regular nano-octahedra was well maintained without obvious change of the size and shape. The TEM images (Figure 1c and d) confirmed that a large number of CuO nanoparticles with an average size of ~70 nm were studded in the interior of octahedral carbon scaffolds. The influence of PVP on the morphology of CuO@C octahedra is also investigated. When the amount of PVP was decreased to 2.0 g, multi-yolk-shell octahedra were still obtained, while no ruggness/bump appeared on the surface (Figure S3a and b). In contrast, porous octahedra derived from pristine $Cu_3(btc)_2$ MOFs without the addition of PVP show a large size of ~15 μm with many CuO nanoparticles attached on the rough surface (Figure S3c and d). The results prove that PVP can suppress the aggregation of CuO nanoparticles and also is favorable for the formation of the CuO@C multi-yolk-shell nanostructures, because PVP was absorbed on the surface of the $Cu_3(btc)_2$ MOFs and then contributed to the formation of porous carbon scaffolds during annealing.

The XRD spectrum of $Cu_3(btc)_2$ MOF/PVP-*4* (Figure S4) clearly shows crystalline diffraction in perfect accordance with the literature [30]. After annealing in N_2 at 700 °C, the characteristic diffraction peaks from Cu_2O and metallic Cu were

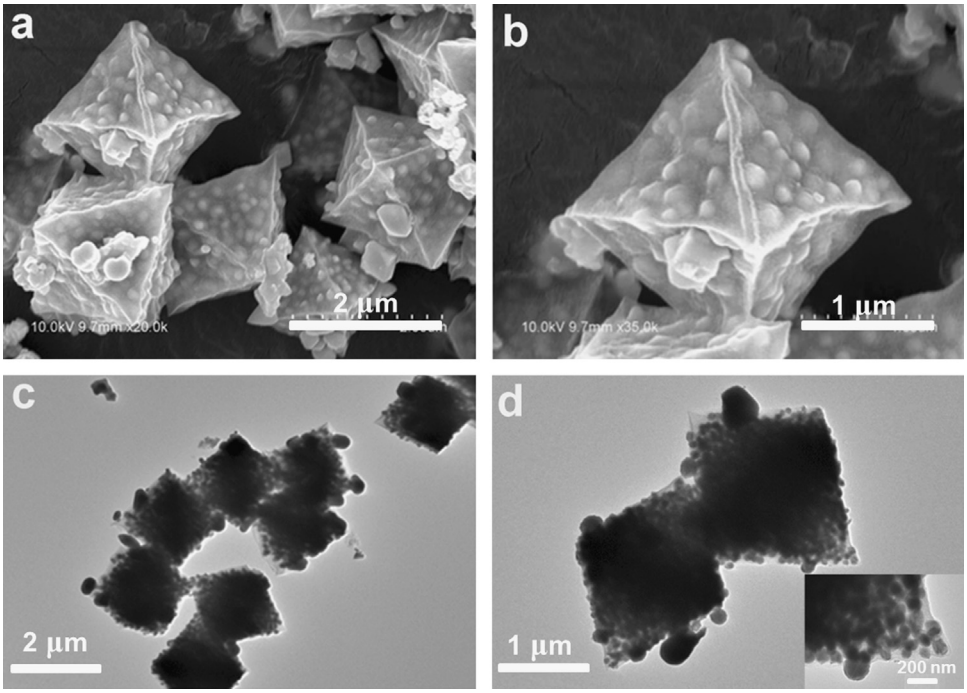

Figure 1 (a,b) SEM and (c,d) TEM images of CuO@C multi-yolk-shell octahedra; (d) the insert shows magnified features of encapsulated CuO nanoparticles near a vertex of a single CuO@C octahedron.

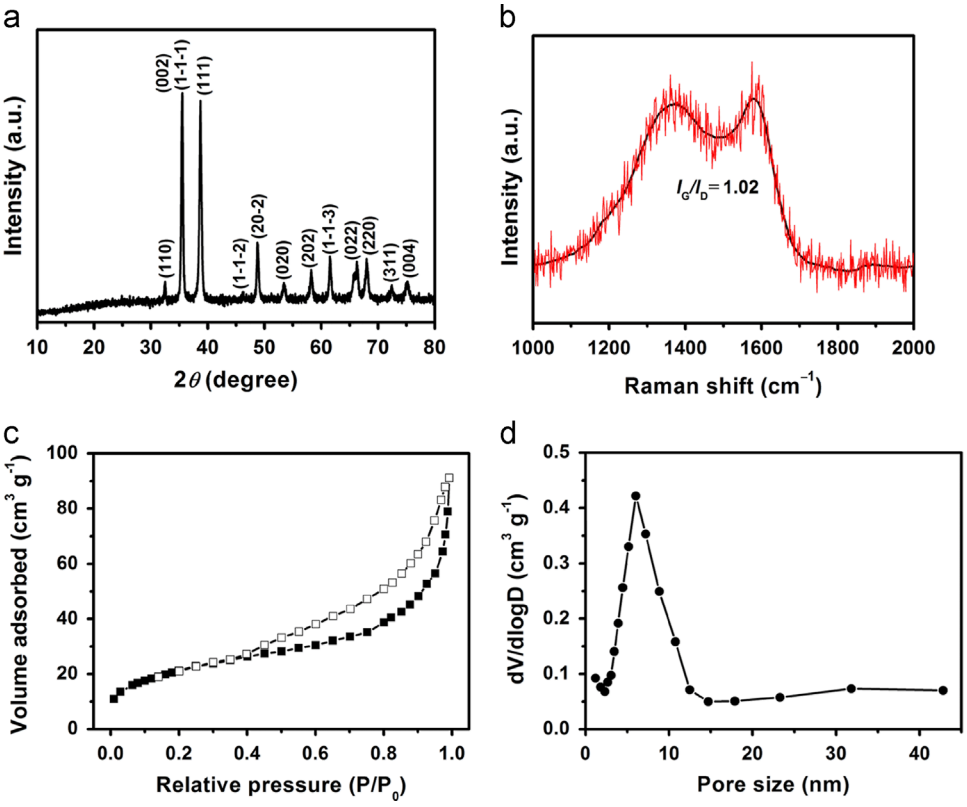

Figure 2 (a) XRD spectrum, (b) Raman spectrum, (c) nitrogen adsorption/desorption isotherms, and (d) pore size distribution of as-prepared CuO@C multi-yolk-shell octahedra.

observed, owing to the formation of massive corresponding nanoparticles in the octahedra. The crystalline structure of CuO@C multi-yolk-shell octahedra was also analyzed by XRD (Figure 2a). All the XRD peaks of CuO@C multi-yolk-shell octahedra can be well assigned to the monoclinic phase of CuO (JCPDS card No. 48-1548, space group *C2/c*, a=4.682,

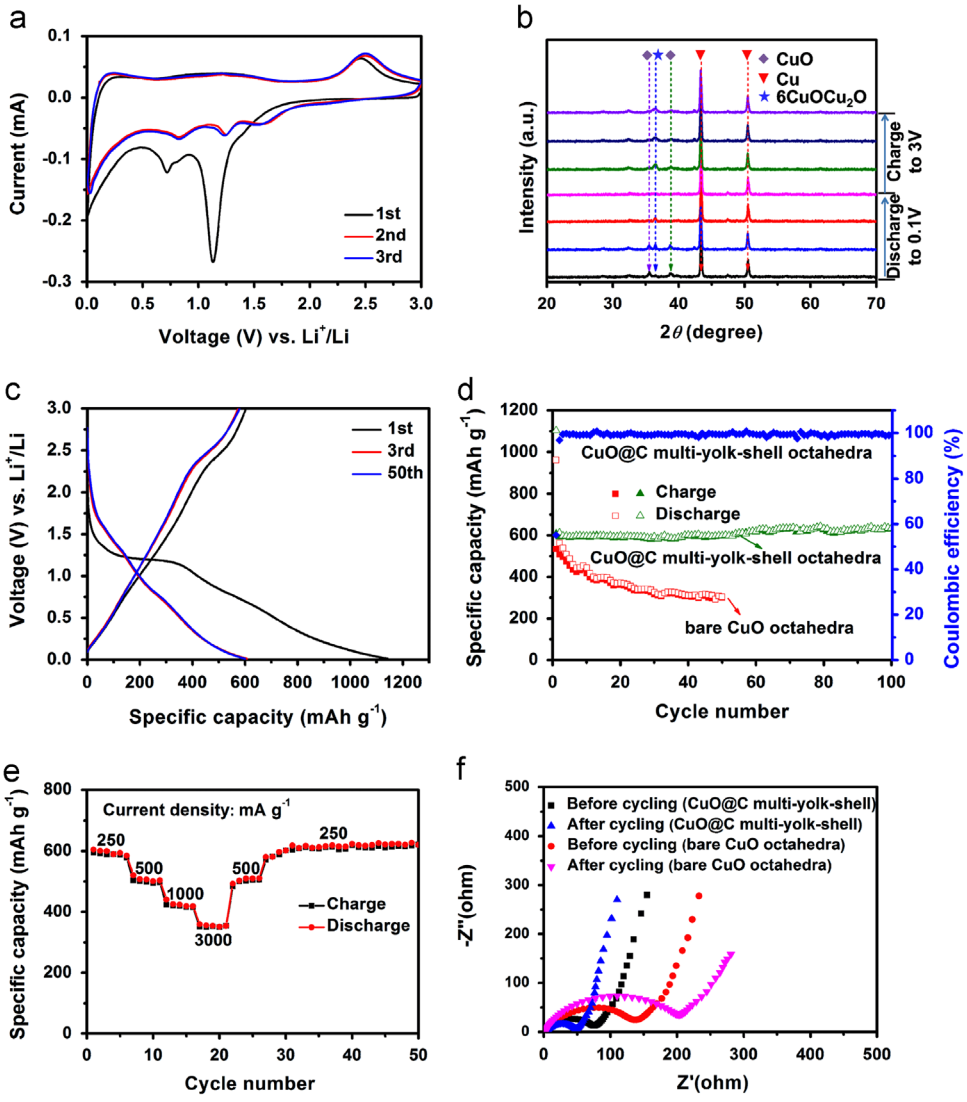

Figure 3 (a) CV curves of CuO@C multi-yolk-shell octahedra at a scan rate of 0.1 mV s^{-1} in the potential range from 0.01 to 3.0 V vs Li/Li^+. (b) Ex-situ XRD spectra of CuO@C multi-yolk-shell octahedra at different charge and discharge states. (c) Charge-discharge curves of CuO@C multi-yolk-shell octahedra at a current density of 250 mA g^{-1}. (d) Cycling performance comparison of CuO@C multi-yolk-shell octahedra and bare CuO octahedra at 500 mA g^{-1}. (e) Rate capability of CuO@C multi-yolk-shell octahedra electrode at different current densities from 250 to 3000 mA g^{-1}. (f) Nyquist plots of CuO@C multi-yolk-shell octahedra and bare CuO octahedra electrodes before and after 50 cycles.

b=3.427, c=5.132). The EDX analysis revealed the presence of Cu, O and C species in the sample (Figure S5). The survey spectrum of XPS was consistent with the above EDX results (Figure S6a). In the high-resolution XPS spectrum of Cu 2p region, the peaks at 933.8 eV (Cu $2p_{3/2}$) and 953.6 eV (Cu $2p_{1/2}$) were observed, owing to the existence of Cu^{2+} [11]. The porous carbon scaffolds encapsulating a lot of CuO nanoparticles can make the octahedral structure significantly robust and tolerant to the large volume change during lithiation/delithiation cycles, which is very beneficial to the performance of LIBs. TGA was utilized to evaluate the carbon content in the products (Figure S7). The weight loss above 350 °C can be mainly ascribed to the oxidation of carbon in air, hence the weight percent of carbon in CuO@C multi-yolk-shell octahedra is evaluated as ~27%. Raman spectroscopy was used to identify the final CuO@C products (Figure 2b). The intensity ratio of G band at 1324 cm^{-1} and D band at 1602 cm^{-1} (I_G/I_D) is calculated to be 1.02, demonstrating that the carbon shells in CuO@C octahedra is amorphous. The porous characteristic of CuO@C multi-yolk-shell octahedra was determined by nitrogen adsorption/desorption analysis and pore size distribution measurement. The isotherm (Figure 2c) displayed a reversible type IV shape between P/P_0=0.45 to 1, attributing to the inner void cavity formed by the partial decomposition of $Cu_3(btc)_2$ MOFs and PVP into gases. The average pore size based on the Barrett-Joyner-Halenda (BJH) method is ~7.0 nm (Figure 2d). The BET surface area and the total pore volume of the porous CuO@C multi-yolk-shell octahedra were measured to be 86 m^2 g^{-1} and 0.14 cm^3 g^{-1}, respectively. Compared to ordinary anode materials, the porous characteristics of CuO@C multi-yolk shell

octahedra can facilitate the mass diffusion of electrolyte and the fast transport of Li^+ as well as buffer the volume variation of CuO nanoparticles, thus giving rise to a high capacity and excellent cycling stability of the electrodes.

For comparison, bare CuO octahedra without carbon shells were also prepared by direct annealing the original $Cu_3(btc)_2$ MOF/PVP-*4* octahedra at 500 °C for 1 h in air. As shown in the SEM images (Figure S8b and c), the as-obtained control sample of bare CuO octahedra also inherited the general appearance of $Cu_3(btc)_2$ MOF/PVP-*4* octahedra, and a large number of CuO nanoparticles stacked into a 3D porous CuO nanostructure. The main difference is that no carbon film is covered on the surface of bare CuO octahedra. Further EDX characterization shows all carbon has been completely removed (Figure S8d). Also, the XRD spectrum of bare CuO octahedra only exhibits typical CuO peaks (Figure S9).

The CV curves of the porous CuO@C multi-yolk-shell octahedra for the first three cycles at a scan rate of 0.1 mV s^{-1} are given in Figure 3a. The first-cycle curve in the cathodic sweep is substantially different from the subsequent curves. In the first cathodic sweep, a well-defined reduction peak is observed at 1.17 V, which is due to the formation of an intermediate Cu_2O phase. Another cathodic peak located at 0.72 V can be ascribed to the decomposition of Cu_2O into Cu and Li_2O [32]. During the subsequent charging process, the anodic peak at 2.47 V corresponds to the oxidation of Cu to Cu_2O and then further oxidation to CuO [12]. The electrochemical reaction involved in the charge–discharge process [33] can be described as:

$$CuO + 2Li^+ + 2e \leftrightarrow Cu + Li_2O \quad (1)$$

Starting from the second cycle, the two cathodic peaks are shifted to 0.8 and 1.25 V with a greatly decreased intensity, whereas the broad anodic peak almost remains unchanged. The CV curves overlap very well from the second cycle onwards, implying good electrochemical reversibility of the CuO@C multi-yolk-shell octahedra.

Ex-situ XRD spectra were employed to further check the phase evolution of CuO at different charge and discharge states within the initial cycle (Figure 3b). The diffraction peaks of CuO at 35.4° and 38.8° gradually disappeared during the discharging process, and a new peak around 36.5° came out, which is assigned to a composite intermediate phase ($6CuOCu_2O$, JCPDS no. 03-0879) [34]. The intermediate phase still exists during the next charging process, while no new characteristic peak is found at the discharging state, suggesting a simple electrochemical reaction process of the electrode.

Figure 3c depicts the first, third, and 50th cycle charge–discharge profiles of the porous CuO@C multi-yolk-shell octahedra at a current density of 250 mA g^{-1} in the voltage range of 0.01 to 3.0 V vs Li^+/Li. There is a plateau at around 1.18 V in the first-cycle discharge curve, owing to the decomposition of CuO into Cu_2O. The initial discharge and charge capacities of the porous CuO@C multi-yolk-shell octahedra electrode are 1140 and 598 mA h g^{-1}, respectively, corresponding to a Coulombic efficiency of 53%. The first-cycle irreversible capacity loss of the CuO@C multi-yolk octahedra is mainly ascribed to the formation of SEI layer, the lithium insertion into carbon scaffolds and the irreversible decomposition of the electrolyte [35,36]. The irreversible capacity loss contributed by amorphous carbon also resulted in the decrease of the first-cycle Coulombic efficiency [37,38]. In the third cycle, the Coulombic efficiency sharply increased to 98%, owing to the stabilization of the SEI film on the outer surface of the carbon scaffolds. Even after 50 cycles, the discharge capacities of the CuO@C multi-yolk-shell octahedra still reached 602 mA h g^{-1}, with almost no fading compared to the second-cycle capacity. Besides, we measured the electrochemical performance of CuO@C multi-yolk-shell octahedra electrode by limiting charge voltage < 1.0 V (as shown in Figure S10).

For comparison, the cycling performance of CuO@C multi-yolk-shell octahedra and bare CuO octahedra at 250 mA g^{-1} is shown in Figure 3d. The CuO@C multi-yolk-shell octahedra electrode delivered a discharge capacity of 1140 mA h g^{-1} and almost no capacity fading was observed after 100 cycles (612 mA h g^{-1} at 100th cycle). In addition, the Coulombic efficiency was maintained at nearly 100%, indicating excellent reversibility. The raising of reversible capacity after a number of cycles has also been reported for many other TMOs, which could be attributed to the reversible formation/dissolution of a polymetric gel-like SEI layer resulting from electrolyte degradation [,39-,41]. On the other hand, the 3D porous carbon matrix strongly enhanced the electrical conductivity of CuO@C multi-yolk-shell octahedra electrode, also prevented the aggregation of CuO nanoparticles during cycling and increased the wettability of electrode materials with electrolyte, thus can greatly improve the cycling performance. In contrast, although the initial discharge capacity of bare CuO octahedra electrode was 962 mA h g^{-1}, the capacity dramatically decreased at the third cycle and reached 300 mA h g^{-1} after 50 cycles.

Moreover, the CuO@C multi-yolk-shell octahedra electrodes also exhibit excellent rate capacity at high current densities (Figure 3e). The capacity retention at the current densities of 250, 500, 1000 and 3000 mA g^{-1} was ranged from 598, 505, 425 to 365 mA h g^{-1}, respectively. A discharge capacity of 610 mA h g^{-1} was attained again upon the reduction of current density to 250 mA h g^{-1}, demonstrating a much better rate performance of the CuO@C multi-yolk-shell octahedra compared to that of the bare CuO octahedra (Figure S11). Furthermore, the reversible capacity of CuO in the CuO@C multi-yolk-shell octahedra was also calculated (as shown in Figure S12).

EIS measurements were conducted to further clarify the electrochemical performances. Figure 3f shows the Nyquist impedance plots of the CuO@C multi-yolk-shell octahedra and bare CuO octahedra electrode before and after 50 cycles. It is found that CuO@C multi-yolk-shell octahedra have a lower charge–discharge resistance (R_{ct}) than bare CuO octahedra before cycling. This proves that the CuO@C multi-yolk-shell octahedra have better electronic conductivity and charge-transfer performance, which should be attributed to the conductive 3D carbon scaffolds. The R_{ct} of the CuO@C multi-yolk-shell octahedra shows an initial resistance of 74 Ω and decreases to 49 Ω after 50 cycles. However, the R_{ct} of the bare CuO octahedra electrode increased from 146 Ω to 206 Ω after 50 cycles. Such intriguing multi-yolk-shell architectures with excellent electron transfer and ion diffusion properties make them as promising anode materials for realizing high capacity and good cycling stability.

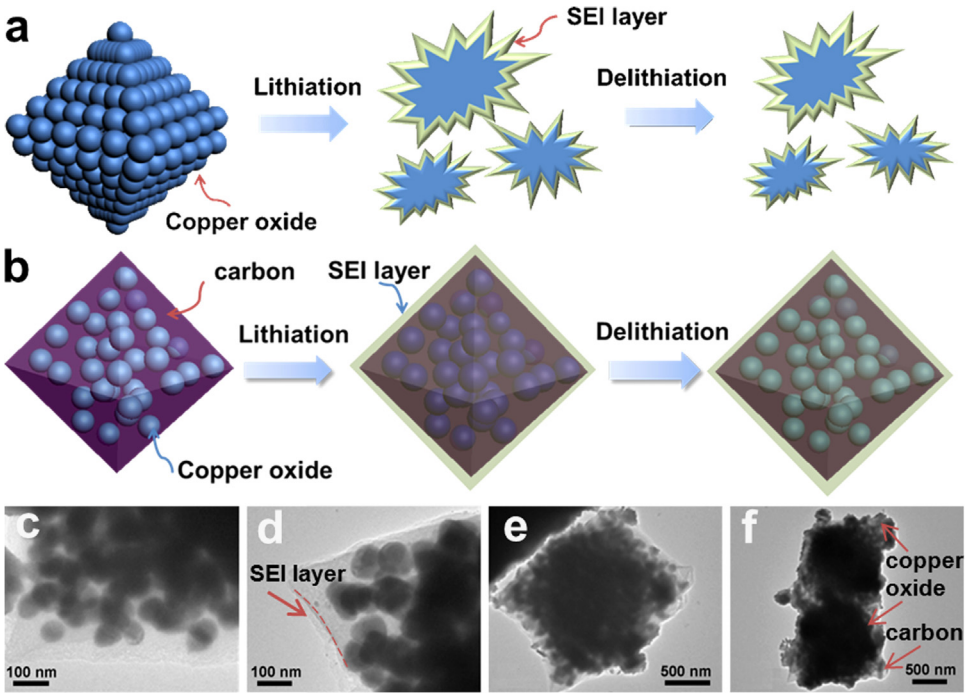

Figure 4 Schematic comparison of the morphological and volumetric changes of (a) bare CuO octahedra and (b) CuO@C multi-yolk-shell octahedra during lithiation/delithiation processes. (c–f) TEM images of CuO@C multi-yolk-shell octahedra (c) before and (d–f) after different amounts of charge–discharge cycles. (d) The thin SEI layer was restricted to the outside of the 3D porous carbon scaffold. (e) The CuO@C multi-yolk-shell octahedra still maintained high structural integrity after 100 cycles at 250 mA g^{-1}. (f) The distribution of carbon shells and CuO nanoparticles at full lithiation state after 300 cycles at 500 mA g^{-1}.

For comparison, the differences in structure integrity of the CuO@C multi-yolk-shell octahedra and bare CuO octahedra after different numbers of charge–discharge cycles were investigated by TEM, as illustrated in Figure 4a and b. Bare CuO octahedra without carbon shell failed to maintain intact octahedral architectures after 50 cycles (Figure S8e), suggesting that the volume variation during the charge/discharge cycles caused structural instability and rapid capacity decay of the bare CuO octahedra electrode. By contrast, the carbon scaffolds in the CuO@C multi-yolk-shell octahedra can buffer the volume change, prevent the aggregation of CuO nanoparticles and restrict the SEI layer to the outside of carbon scaffolds (Figure 4c–f). The conductive carbon shell acted as a barrier for the formation of most SEI film (Figure 4d). Well-preserved carbon shells and CuO cores were still observed after 100 cycles (Figure 4e). Upon full lithiation state after 300 cycles at 500 mA g^{-1}, the volume expansion of CuO cores reached a maximum value but still could not break the carbon scaffolds (Figure 4f). These results prove that the conductive 3D carbon networks with excellent structural stability can keep the electrode intact during long-term cycling, which is very beneficial to the cycle life.

The long-term cycling performance of CuO@C multi-yolk-shell octahedra at 500 mA g^{-1} is shown in Figure 5. The initial discharge and charge capacities are 905 and 515 mA h g^{-1} respectively. After a few charge–discharge cycles, the CuO@C multi-yolk-shell octahedra electrode exhibited excellent cycling stability and finally reached a capacity of 512 mA h g^{-1} after 300 cycles, and the capacity retention measured from the second cycle is as high as 97%. It proves that the wrapping of the CuO nanoparticles within conductive 3D carbon scaffolds can prevent the degradation of the electrochemical performance after long cycles. Therefore, the CuO@C multi-yolk-shell octahedra presented outstanding charge–discharge cyclability.

To verify the potential for practical application, the CuO@C multi-yolk-shell octahedra anodes and commercial $LiFePO_4$ cathodes were assembled into full cells. The rate performance of commercial $LiFePO_4$ powder cathode is shown in Figure 6a. The commercial $LiFePO_4$ powder exhibited a reversible specific capacity of 129 mAh·g^{-1} at 0.5 C (1C=170 mA g^{-1}). When the current density increased to 4 C, the capacity decreased to ~70 mA h g^{-1}. Figure 6b displays the charge–discharge curve of the CuO@C/$LiFePO_4$ full cell at a rate of 0.1 C cycling between 0.9–4.0 V. The full cell delivers an initial discharge and charge capacities of 109 and 113 mA h g^{-1}, respectively, corresponding to an initial Coulombic efficiency of 96%. Obviously, the pre-lithiation process of anode electrode significantly improved the Coulombic efficiency of the CuO@C/$LiFePO_4$ full cell. The rate capability of a full cell with CuO@C multi-yolk-shell octahedra anode and $LiFePO_4$ cathode is depicted in Figure 6c. The capacities of full cell were calculated to be 109, 95, 74, 50 mA h $g^{-1}_{LiFePO4}$ at 0.5 C, 1C, 2C and 4C, respectively. On the basis of the loading mass of CuO@C multi-yolk-shell octahedra, the full cell delivered the discharge capacities of 326, 281, 220, 150 mA h $g^{-1}_{CuO@C}$, respectively. The cycling stability of above full cells was also investigated (Figure 6d). The full cell showed slightly decreased capacity from 109 to 99 mA h $g^{-1}_{LiFePO4}$ after 100

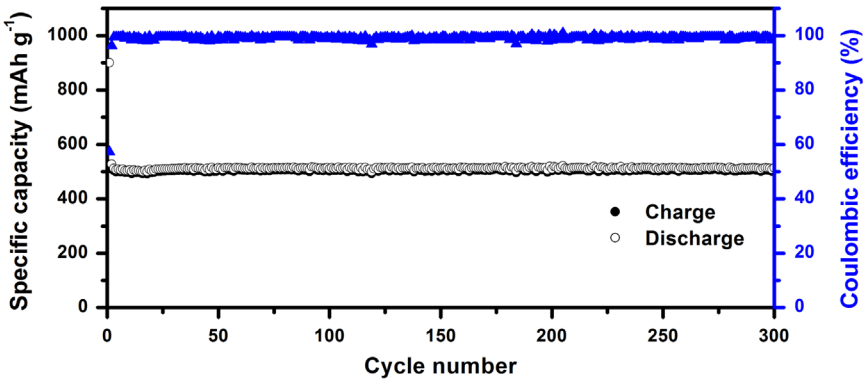

Figure 5 Cycling performance of CuO@C multi-yolk-shell octahedra electrode at 500 mA g^{-1} for 300 cycles.

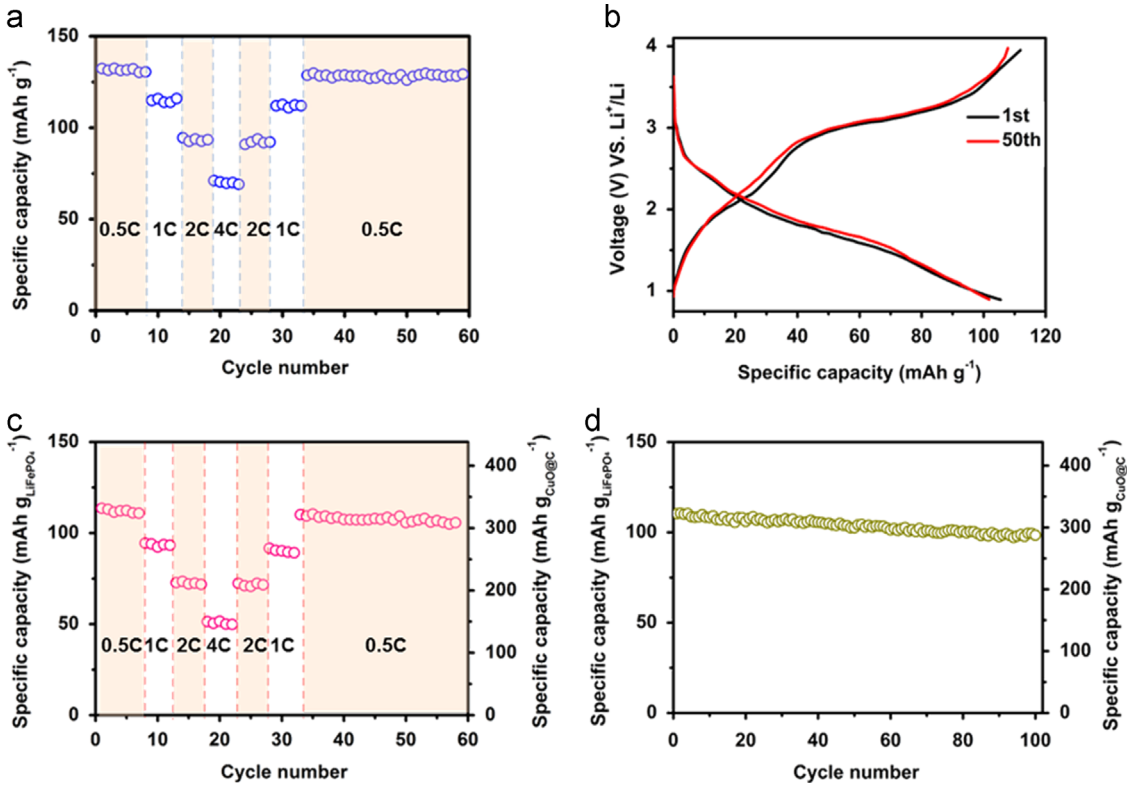

Figure 6 (a) Rate capability of commercial $LiFePO_4$ powder cathode at different current rates. (b) Charge–discharge curve of CuO@C/$LiFePO_4$ full cell at a rate of 0.1 C. (c) Rate capability of CuO@C/$LiFePO_4$ full cell at different current rates. (d) Cycling performance of CuO@C/ $LiFePO_4$ full cell at 0.5 C for 100 cycles.

cycles based on the mass of $LiFePO_4$ at a current density of 0.5 C, corresponding to a capacity retention of 91%. Similarly, this full cell exhibited the first discharge capacity of 326 mA h $g^{-1}_{CuO@C}$ and 296 mA h $g^{-1}_{CuO@C}$ after 100 cycles, which was calculated by the loading mass of CuO@C multi-yolk-shell octahedra. These results confirmed that the full cell can retain high capacity for numerous cycles, indicative of the chemical robustness of the electrodes. The performance of full cell is mostly limited by commercial $LiFePO_4$ cathode, rather than CuO@C multi-yolk-shell octahedra anode. Considering their facile synthesis, well-defined structure, and high cyclability performance, CuO@C multi-yolk-shell octahedra are promising for practical application of lithium ion batteries with long life and high stability.

Conclusions

In summary, we have rationally designed and synthesized a novel CuO@C multi-yolk-shell octahedra composite structure via a simple solvothermal method and a two-step annealing process. Compared to the bare CuO octahedra, the CuO@C multi-yolk-shell octahedra electrodes demonstrated a much better capacity retention, excellent cycling stability and rate capability. It proves that the 3D porous and conductive carbon scaffolds of the CuO@C multi-yolk-shell octahedra can greatly improve the reversible capacity, rate performance and long-term cyclability. In addition to CuO, we expect that the feasible synthesis strategy in this work could be extended to prepare other multi-yolk-shell-structured TMO/carbon composites for

the application of next-generation LIBs and other energy storage devices.

Acknowledgments

This work is supported by the National Thousand Young Talents Program of China, the Young Scientists Project of National Basic Research Program of China (973 Program no. 2015CB659300), the National Natural Science Foundation of China (NSFC Grant nos. 21403105 and 21573108), the China Postdoctoral Science Foundation (Grant nos. 2015M581769 and 2015M580408), the Natural Science Foundation for Young Scholars of Jiangsu Province (Grant nos. BK20150571 and BK20150583), the Fundamental Research Funds for the Central Universities and a project funded by the Priority Academic Program Development of Jiangsu Higher Education Institutions (PAPD).

Appendix A. Supplementary material

Supplementary data associated with this article can be found in the online version at http://dx.doi.org/10.1016/j.nanoen.2015.12.024.

References

[1] Y. Gogotsi, ACS Nano 8 (2014) 5369–5371.
[2] K. Amine, R. Kanno, Y.H. Tzeng, MRS Bull. 39 (2014) 395–405.
[3] N.S. Choi, Z.H. Chen, S.A. Freunberger, X.L. Ji, Y.-K. Sun, K. Amine, G. Yushin, L.F. Nazar, J. Cho, P.G. Bruce, Angew. Chem. Int. Ed. 51 (2012) 9994–10024.
[4] S. Chaudhari, M. Srinivasan, J. Mater. Chem. 22 (2012) 23049–23056.
[5] R. Sahay, P.S. Kumar, V. Aravindan, J. Sundaramurthy, W. C. Ling, S.G. Mhaisalkar, S. Ramakrishna, S. Madhavi, J. Phys. Chem. C 116 (2012) 18087–18092.
[6] N.A. Barakat, M.S. Khil, F.A. Sheikh, H.Y. Kim, J. Phys. Chem. C 112 (2008) 12225–12233.
[7] L. Li, A.R.O. Raji, J.M. Tour, Adv. Mater. 25 (2013) 6298–6302.
[8] C. Wang, D. Higgins, F.F. Wang, D.Y. Li, R.Q. Liu, G.F. Xia, N. Li, Q. Li, H. Xu, G. Wu, Nano Energy 9 (2014) 334–344.
[9] T. Wen, X.L. Wu, S. Zhang, X. Wang, A.W. Xu, Chem. Asian J. 10 (2015) 595–601.
[10] S. Ko, J.I. Lee, H.S. Yang, S. Park, U. Jeong, Adv. Mater. 24 (2012) 4451–4456.
[11] Y. Liu, W. Wang, L. Gu, Y.W. Wang, Y. Ying, Y.Y. Mao, L.W. Sun, X.S. Peng, ACS Appl. Mater. Interfaces, 5, 9850–9855.
[12] J.C. Park, J. Kim, H. Kwon, H. Song, Adv. Mater. 21 (2009) 803–807.
[13] Y.M. Zhang, W.X. Zhang, M. Li, Z.H. Yang, G.D. Chen, Q. Wang, J. Mater. Chem. A 1 (2013) 14368–14374.
[14] L. Zhang, H.B. Wu, S. Madhavi, H.H. Hng, X.W. Lou, J. Am. Chem. Soc. 134 (2012) 17388–17391.
[15] L. Zhang, H.B. Wu, X.W. Lou, J. Am. Chem. Soc. 13 (2013) 10664–10672.
[16] R.B. Wu, X.K. Qian, X.H. Rui, H. Liu, B.L. Yadian, K. Zhou, J. Wei, Q.Y. Yan, X.Q. Feng, Y. Long, L.Y. Wang, Y. Huang, Small 10 (2014) 1932–1938.
[17] H.L. Jiang, Q. Xu, Chem. Commun. 47 (2011) 3351–3370.
[18] X.D. Xu, R.G. Cao, S.Y. Jeong, J. Cho, Nano Lett. 12 (2012) 4988–4991.
[19] R.B. Wu, X.K. Qian, F. Yu, H. Liu, K. Zhou, J. Wei, Y.Z. Huang, J. Mater. Chem. A 1 (2013) 11126–11129.
[20] L. Hu, Y. Huang, F. Zhang, Q. Chen, Nanoscale 5 (2013) 4186–4190.
[21] R. Wu, X. Qian, K. Zhou, J. Wei, J. Lou, P.M. Ajayan, ACS Nano 8 (2014) 6297–6303.
[22] F. Zou, X.L. Hu, Z. Li, L. Qie, C.C. Hu, R. Zeng, Y. Jiang, Y. Huang, Adv. Mater. 26 (2014) 6622–6628.
[23] Z.Y. Cai, L. Xu, M.Y. Yan, C.H. Han, L. He, K.M. Hercule, C.J. Niu, Z.F. Yuan, W.W. Xu, L.B. Qu, K.N. Zhao, L.Q. Mai, Nano Lett. 15 (2014) 738–744.
[24] J.N. Zhang, K.X. Wang, Q. Xu, Y.C. Zhou, F.Y. Cheng, S.J. Guo, ACS Nano 9 (2015) 3369–3376.
[25] H.W. Zhang, L. Zhou, O. Noonan, D.J. Martin, A.K. Whittaker, C.Z. Yu, Adv. Funct. Mater. 24 (2014) 4337–4342.
[26] N. Liu, H. Wu, M.T. McDowell, Y. Yao, C. Wang, Y. Cui, Nano Lett. 12 (2012) 3315–3321.
[27] H. Wu, G. Zheng, N. Liu, T.J. Carney, Y. Yang, Y. Cui, Nano Lett. 12 (2012) 904–909.
[28] N. Liu, Z.D. Lu, J. Zhao, M.T. McDowell, H.-W. Lee, W.T. Zhao, Y. Cui, Nat. Nanotech 9 (2014) 187–192.
[29] B. Wang, X.L. Li, X.F. Zhang, B. Luo, Y.B. Zhang, L.J. Zhi, Adv. Mater. 25 (2013) 3560–3565.
[30] A. Banerjee, U. Singh, V. Aravindan, M. Srinivasan, S. Ogale, Nano Energy 2 (2013) 1158–1163.
[31] J. Hassoun, F. Bonaccorso, M. Agostini, M. Angelucci, M.G. Betti, R. Cingolani, M. Gemmi, C. Mariani, S. Panero, V. Pellegrini, B. Scrosati, Nano Lett. 14 (2014) 4901–4906.
[32] N. Pereira, L. Dupont, J.M. Tarascon, L.C. Klein, G.G. Amatucci, J. Electrochem. Soc. 150 (2003) A1273–A1280.
[33] Y. Zhang, M.W. Xu, F. Wang, X.P. Song, Y.H. Wang, S. Yang, J. Phys. Chem. C 117 (2013) 12346–12351.
[34] S. Yuan, X.L. Huang, D.L. Ma, H.G. Wang, F.Z. Meng, X.B. Zhang, Adv. Mater. 26 (2014) 2273–2279.
[35] Y. Chen, B.H. Song, M. Li, L. Lu, J.M. Xue, Adv. Funct. Mater. 24 (2014) 319–326.
[36] J.S. Luo, J.L. Liu, Z.Y. Zeng, C.F. Ng, L.J. Ma, H. Zhang, J.Y. Lin, Z.X. Shen, H.J. Fan, Nano Lett. 13 (2013) 6136–6143.
[37] Y.P. Wu, E. Rahm, R. Holze, J. Power Sources 114 (2003) 228–236.
[38] M. Rahman, J.Z. Wang, M.F. Hassan, D. Wexler, H.K. Liu, Adv. Energy Mater. 1 (2011) 212–220.
[39] Z.Y. Wang, F.B. Su, S. Madhavi, X.W. Lou, Nanoscale 3 (2011) 1618–1623.
[40] L.L. Wang, H.X. Gong, C.H. Wang, D.K. Wang, K.B. Tang, Y.T. Qian, Nanoscale 4 (2012) 6850–6855.
[41] S. Laruelle, S. Grugeon, P. Poizot, M. Dollé, L. Dupont, J.M. Tarascon, J. Electronchem. Soc. 149 (2002) A627–A634.

Dr. Tao Chen received his Ph.D. degree in Chemical Engineering and Technology under supervision of Prof. Jiajun Fu from Nanjing University of Science and Technology in June 2015. He is currently a postdoctoral researcher in the group of Prof. Zhong Jin at Nanjing University. His current research focuses on the design and synthesis of nanostructured electrode materials for sodium and lithium ion batteries.

Yi Hu received his B.S. degree in chemistry from Sichuan University in 2014. He is now pursuing his M.S. degree under the supervision of Professor Zhong Jin in School of Chemistry and Chemical Engineering at Nanjing University. His research interests reside in two-dimensional nanomaterials for electrochemical energy storage and photoelectric conversion.

Baorui Cheng entered School of Chemistry and Chemical Engineering, Nanjing University in 2013. He majors in chemistry and currently works as an assistant of Dr. Tao Chen in the group of Prof. Zhong Jin. His current research focuses on preparation of MOFs-based functional materials.

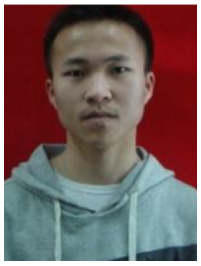

Renpeng Chen has graduated from the Northeastern University (China) since 2014. Now, he is pursuing his M.S. degree under the guidance of Professor Zhong Jin in School of Chemistry and Chemical Engineering at Nanjing University. His research interest is focused on the synthesis of alloy materials for lithium ion batteries.

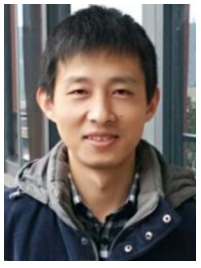

Dr. Hongling Lv received his Ph.D. degree in Materials Processing Engineering under supervision of Professor Jieming Cao from Nanjing University of Aeronautics and Astronautics (2014). He is currently a postdoctoral researcher in the group of Prof. Zhong Jin at Nanjing University. His current research activities focus on key materials for lithium-ion batteries, lithium-sulfur batteries and lithium-selenium batteries.

Lianbo Ma received his M.S. degree in Applied Chemistry from Jiangsu University, PR China (2015). He is now pursing his PhD degree under the supervision of Prof. Zhong Jin and Jie Liu in School of Chemistry and Chemical Engineering, Nanjing University, PR China. His main interest is the design and fabrication nanomaterials for energy storage, electrochemistry, and photoelectric conversion.

Guoyin Zhu obtained his M.S. degree from Nanjing University of Posts & Telecommunications in 2014. Currently, he is pursuing his Ph.D. degree under the supervision of Prof. Zhong Jin and Jie Liu at Nanjing University. His research is mainly focused on the synthesis of carbonaceous nanomaterials, and their application for energy conversion and storage devices.

Yanrong Wang received her master degree in physical chemistry under the supervision of Professor Yong Hu in College of Chemistry and life sciences at Zhejiang Normal University in 2015. She is now pursuing her Ph. D. degree under the supervision of Professor Zhong Jin in School of Chemistry and Chemical Engineering at Nanjing University. Her current research interest is the design of new type of battery.

Dr. Changzeng Yan received his Ph.D. degree from Sungkyunkwan University in Korea in August of 2014 under the supervision of Prof. Dae Joon Kang. He is currently working as a postdoctoral research fellow in Prof. Zhong Jin's research group at School of Chemistry and Chemical Engineering, Nanjing University. His research intersts include designing and fabrication of novel photocatalyst for solar energy conversion applications: water splitting, CO_2 reduction, and N_2 fixation. He aims to employ varieties of synergistic effects resulting from nanoherostructures to enhance the energy conversion efficiency.

Dr. Zuoxiu Tie received her B.S. (2004) degree and Ph.D. (2010) from Nanjing University. She is currently a research assistant in the group of Prof. Zhong Jin. Her current research interest focuses on carbonaceous nanomaterials for energy conversion and storage devices.

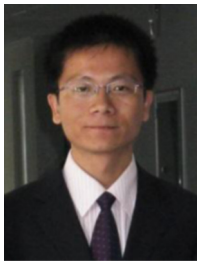

Prof. Zhong Jin received his B.S. (2003) and Ph.D. (2008) in chemistry from Peking University. He worked as a postdoctoral scholar at Rice University and Massachusetts Institute of Technology. Now he is a professor in School of Chemistry and Chemical Engineering at Nanjing University. He leads a research group working on functional nanomaterials and devices for energy conversion and storage.

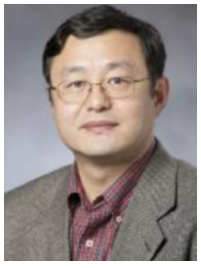

Prof. Jie Liu is currently the George B. Geller Professor of Chemistry at Duke University and an adjunct professor of "Thousands Talents" Program at Nanjing University. He earned a B.S. from Shandong University in 1987 and a PhD from Harvard University in 1996. His research interests include the synthesis and chemical functionalization of nanomaterials, nanoelectronic devices, scanning probe microscopy, and carbon nanomaterials. Prof. Liu is a Fellow of the AAAS, APS and RSC.